

## Measuring the Content of Unfrozen Water in Frozen Soil Based on Resistivity

Liyun Tang<sup>1</sup>, Xin Wang<sup>1,\*</sup>, Fangyan Lan<sup>1</sup>, Peiyong Qiu<sup>2</sup>, Long Jin<sup>1,3</sup>

<sup>1</sup> School of Architecture and Civil Engineering, Xi'an University of Science and Technology, Xi'an, Shanxi 710054, China

<sup>2</sup> Department of Civil, Geological, and Mining Engineering, École Polytechnique de Montréal, Research Institute on Mines and Environment (RIME) UQAT-Polytechnique, Montréal, QC H3C 3A7, Canada

<sup>3</sup> CCCC First Highway Consultants Co., Ltd, Xi'an Shanxi 710000, China

\*E-mail: [wangxindeli@163.com](mailto:wangxindeli@163.com)

Received: 10 May 2020 / Accepted: 3 July 2020 / Published: 10 August 2020

---

This study proposes a new method for calibrating the theoretical model of resistivity versus unfrozen water content in frozen soils. The method characterizes correlations between the soil mass resistivity and unfrozen water content in the frozen state by investigating the relation between resistivity and liquid water content in the drying state. The essential similarity between the soil mass freezing and drying processes is analyzed through the process and path of unfrozen (liquid) water reduction. The resistivity and unfrozen water (liquid water) content were correlated in soil samples with different particle sizes (clay, silt, and sandy soil) during freezing and drying. The test results showed that during freezing to temperatures below 5 °C (clay), 4 °C (silt), and 3 °C (sandy soil), the unfrozen water content thresholds of providing directional migration channels for conducting particles were 17%, 14%, and 13%, respectively. During drying, the threshold water contents of clay, silt, and sandy soil were 15.35%, 14.87%, and 14.34%, respectively. The correlation between the soil resistivity ( $\rho_D$ ) and unfrozen water content ( $\theta_u$ ) in the freezing process can be expressed based on that between the soil resistivity and liquid water content in the drying state. Thus, the theoretical model of unfrozen water content can be calibrated by conducting a resistivity test under the drying condition. This new method is suitable for model calibrations of electrical resistance tomography for engineering applications in cold regions.

---

**Keywords:** Unfrozen water; Soil resistivity; NMR; Freezing; Drying

### 1. INTRODUCTION

Geotechnical engineers often determine the liquid water content in soil from soil resistivity variations [1-4]. The resistivity test results with respect to the soil volume water content are less

erroneous than those obtained using the standard method [5, 6]. In frozen soil areas, high-resistivity layers are formed on the soil surface after freezing. Changes in the environmental temperature can change the resistivity values by tens or hundreds of times [7]. The distribution of underground frozen soil has been investigated with some success by geophysical exploration methods. For example, Alekseev [8] detected the limit of frozen soil distribution in the south and north along the Xinjiang–Tibet Highway with electrical sounding, and determined the thickness of the frozen soil layer. Keuschnig [9] monitored the stability of rock slopes in the Zugspitze region by electrical resistance tomography (ERT). In their studies, the main technical purpose of ERT was analyzing the change of unfrozen water content in rock fractures. Drahor [10] tested the distribution of underground caverns using ERT, and discussed the applicability of ERT in soils with different water contents.

Accurately determined correlations between field soil resistivity and unfrozen water content ( $\rho_D - \theta_u$  correlations) in frozen soils are the basis of ERT engineering applications in cold regions. Although resistivity tests in geophysics are relatively mature, the development of testing methods for unfrozen water content has bottlenecked the development of calibration models.

The physical and mechanical characteristics of the frozen soil are dependent on the presence of unfrozen water; therefore, determining its content is particularly important [11-14]. Currently, the unfrozen water content in frozen soils can be detected by several methods. Time domain reflectometry is simple and clear, but the applicability of its calibration curve is debatable [15-20]. The calorimetric method based on the energy conservation law operates by a simple principle, but requires a complex calculation process [21]. Nuclear magnetic resonance (NMR) is an early and mature technique for testing the unfrozen water content in frozen soil [22]. This technology provides a relational model between the unfrozen water content and the soil temperature. The influencing factors of unfrozen water content in frozen soils have been determined under different soil conditions, yielding important results [23]. However, NMR technology is limited to laboratory measurements, and the test cost is high [24]. Considering the mature development of ERT, obtaining the unfrozen water content in frozen soils from the variations in frozen soil resistivity is a feasible prospect [25]. However, during the field test, the correlation between the resistivity and the unfrozen water content of the soil samples must be determined for calibrating the unfrozen water content model. In establishing such a relation, the temperature variable can be considered as a bridge linking the resistivity to the frozen water content. The correlations between temperature and resistivity and between temperature and the unfrozen water content can then be established. The former can be obtained through resistivity testing equipment. However, scholars have always believed that the correlation between temperature and unfrozen water content can be more accurately determined by NMR, which requires costly equipment. Therefore, the feasibility of the sample size and the test cost must both be considered when calibrating a theoretical model in the field. In particular, the calibration results obtained from many samples should ensure the accuracy and scientific integrity of the theoretical model.

Against this background, a method that quickly calibrates the resistivity and unfrozen water content is urgently demanded. Based on the influence rule of liquid water content on soil resistivity, this study experimentally tests the correlation between the soil mass resistivity and liquid water content of the soil under freezing and drying conditions. Combining a theoretical analysis and test results, it then proposes a new method that characterizes the correlation between the soil mass resistivity and

unfrozen water content in the frozen state from the relation between the soil mass resistivity and water content in the drying state. This method is suitable for calibrating test models in ERT engineering applications in cold regions.

## 2. EXPERIMENTAL

### 2.1. Materials

In this paper, the correlations between resistivity and liquid water content in frozen and dried soils were investigated in three kinds of soil materials with different particle sizes (sandy soil, silt, and clay). The soil samples were prepared from loess and sandy soil in the Xi'an area. The samples were collected, air-dried, and crushed prior to testing. The particle size distributions of the soil test samples were measured by a laser particle size analyzer (Bettersize 2000; Liaoning, China). The physical parameters of the tested soil are shown in Table 1.

**Table 1.** Basic physical parameters of the tested soils

Category	Sandy soil	Silt	Clay
	97% sand grains	7% sand grains	8% sand grains
Composition	2% powder particles	84% powder particles	41% powder particles
	1% clay fractions	9% clay fractions	51% clay fractions
Liquid limit	-	27.8%	75.5%
Plastic limit	-	25.4%	24.9%
Plasticity index	-	1.4%	50.6%
Volume weight	2.67	2.72 (no test-predicted value)	2.83

The appropriate amount of each soil sample was weighed and placed in a cuboid glass plate (inner dimensions  $[30 \times 15 \times 5] \text{ cm}^3$ ). Following the Wilson's test method [26], the tested soils were prepared with a pre-set initial water content (25% sandy soil, 30% silt, and 60% clay) by adding the appropriate amount of water to the soil sample. The obtained sample should have a simple initial state and a uniform internal structure. Wilson's method is intended to reduce the cost of repeated testing and facilitate result analysis. Each prepared soil mass was sealed in a plastic bag for 72 h to ensure stable and uniform moisture diffusion. The soil samples in the plate were cut into soil test samples for placement in the Mile soil sample box (inner dimensions  $[15 \times 5 \times 5] \text{ cm}^3$ ; Fig. 1). Conducting strips were deployed on the left and right sides of the soil sample box in close contact with the soil samples. Four temperature holes were observed on the front and back walls of the soil sample box. Into each temperature hole, a temperature sensor probe was inserted to a depth of 2 cm.

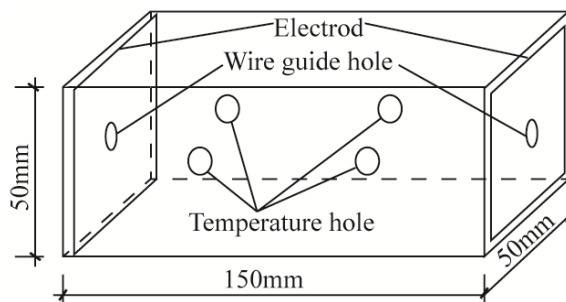


**Figure 1.** Soil sample box

The main equipment of the freezing test was a low-temperature NMR microstructural analysis system (MacroMR12-150; Jiangsu, China), which detected the correlation between the unfrozen water content and temperature in the frozen soil. The auxiliary equipment included an AC-voltage regulating power supply (STG-500W; Zhejiang, China), a voltmeter (UT-201; Shanghai, China), a multimeter supporting low-temperature systems (VC9806; Guangdong, China), and a four-channel temperature monitoring system (HT-9815; Guangdong, China, with a test accuracy of  $\pm 0.1$  °C). The main equipment of the drying test was a vacuum drying oven (temperature range: 10 °C~300 °C, control accuracy: 0.1 °C), supported by a voltage controlled power source (STG-500W AC), a voltmeter (UT-201), a multimeter (VC9806) and an electronic scale with a test accuracy of 0.01 g.

2.2. Methods

Clay, silt, and sandy soils with different particle sizes were tested in this study. The resistivity, unfrozen water content, and temperature correlations were measured in 12 frozen soil samples. Four test samples were prepared for each type of soil mass: two (parallel control) samples for the resistivity test and two (parallel control) samples for the unfrozen water content. The initial water content was re-measured after preparing the soil samples. Six samples were prepared for testing the correlation between the liquid water content of the soil and the resistivity in the dried state. Two samples of each kind of soil were prepared as the parallel control. The specific test groups are shown in Table 2.

**Table 2.** Test groups for obtaining correlations between the frozen soil temperature, resistivity, and unfrozen water content

Soil mass type	No.	Initial water content	Test environment	Data collection frequency	Test index
Clay	C1	58.0%	Deep freezing	1 °C/time	$\theta, T$
	C2	57.1%	Deep freezing	1 °C/time	$\theta, T$
	C3	59.4%	Deep freezing	1 °C/time	$\rho, T$
	C4	58.1%	Deep freezing	1 °C/time	$\rho, T$
	C5	59.4%	Drying at 45 °C	4 min/time	$\rho, \theta, t$

Silt	C6	58.1%	Drying at 45 °C	4 min/time	$\rho, \theta, t$
	M1	29.7%	Deep freezing	1 °C/time	$\theta, T$
	M2	30.1%	Deep freezing	1 °C/time	$\theta, T$
	M3	30.7%	Deep freezing	1 °C/time	$\rho, T$
	M4	30.1%	Deep freezing	1 °C/time	$\rho, T$
	M5	30.7%	Drying at 45 °C	2 min/time	$\rho, \theta, t$
Sandy soil	M6	30.1%	Drying at 45 °C	2 min/time	$\rho, \theta, t$
	S1	25.0%	Deep freezing	1 °C/time	$\theta, T$
	S2	25.5%	Deep freezing	1 °C/time	$\theta, T$
	S3	25.1%	Deep freezing	1 °C/time	$P, T$
	S4	25.4%	Deep freezing	1 °C/time	$\rho, T$
	S5	25.1%	Drying at 45 °C	2 min/time	$\rho, \theta, t$
	S6	25.4%	Drying at 45 °C	2 min/time	$\rho, \theta, t$

Note:  $\rho$  is the resistivity,  $\theta$  is the unfrozen water content, and  $t$  is the test time.

$\theta$  was determined by NMR as described in the literature [17] and was calculated as follows:

$$\theta_u = \theta_0 \frac{Y_s}{Y_n} \quad (1)$$

where  $\theta_u$  and  $\theta_0$  are the unfrozen and initial water contents, respectively,  $Y_s$  is the signal strength, and  $Y_n$  is the signal strength at a certain temperature obtained by a paramagnetic linear regression function.

The soil resistivity was calculated by Eq. (2) [19].

$$\rho = \frac{U \cdot S}{I \cdot L} \quad (2)$$

where  $U$  is the voltage,  $I$  is the current, and  $S$  and  $L$  are the lateral area and length of the tested soil sample, respectively.

The correlation between the unfrozen water content and temperature of the frozen soil was determined by the following process. First, the prepared soil sample was placed in a low-temperature thermostat bath connected to a conductor. The soil test sample was frozen at  $-30$  °C. The signal and resistivity of the hydrogen atom were measured as the soil temperature was lowered by 1 °C intervals. The measurement frequency was appropriately increased when the temperature reached 0 °C and below. The total freezing time of the test was at least 12 h, and the temperature control was based on the readings of the sensor probe inserted into the soil sample (the soil temperature was taken as the average of the temperatures at four points).

The process for testing the correlation between frozen soil resistivity and temperature is described as follows: A prepared soil sample is placed in the same low-temperature environment as in the unfrozen water content test process outlined above (the low-temperature environment box consists of a standard NMR equipment coil and insulation material cooled by cold liquid). The conductors on each side of the soil sample box are fixed with a conducting strip. The soil sample is cooled to a freezing temperature of  $-30$  °C, and voltage and current data are recorded each time the temperature is lowered from this initial temperature by 1 °C. Voltage is controlled at  $50 \text{ V} \pm 1 \text{ V}$ , and the test equipment's temperature control is based on readings from a temperature sensor inserted into the soil sample (temperatures at four points are selected to calculate an average value).

The specific steps for testing resistivity and water content during drying are as follows: First, the conductor is connected, then the soil sample is placed on the electronic scale bracket, and the bracket mass and initial soil sample mass are recorded. Next, the drying baker temperature is adjusted to keep it at the pre-set temperature ( $\pm 3$  °C). The drying time is then determined in combination with the description of the pre-test results and is combined with the liquid water loss rate during soil sample drying. The soil sample resistivity and mass are tested based on the test timings presented in Table 2. To ensure test accuracy, the test circuit's power supply should then be turned off each time the resistivity is recorded.

During the soil sample drying process, soil sample resistivity and soil mass variation are tested based on the set time, and the liquid water content under each test node is converted following a conversion formula that can be expressed as

$$\theta = \frac{D - B - C}{C} \times 100\% \quad (3)$$

where  $B$  is the soil sample bracket mass (g),  $D$  is the residual mass (g), and  $C$  is the total dry soil mass (g) of the soil sample determined using the formula of  $C = (A - B)(1 + \omega)$ , where  $A$  is the soil sample's initial mass (g) and  $\omega$  is its initial water content (%).

### 3. RESULTS AND DISCUSSION

#### 3.1. Relation between unfrozen water content and temperature

The correlation between temperature and unfrozen water content in case of the sandy (S1), silt (M1), and clay (C1) soils based on NMR is presented in Fig. 2. The test results in the parallel control group show good consistency, thus the test results of the unfrozen water content of samples C1, M1, and S1 with varying temperatures variation are analyzed correctly.

Below 0 °C, unfrozen water content clearly decreased with the decreasing temperature, whereas the unfrozen water content remained almost unchanged in the positive temperature stage. For C1, the unfrozen water content decreases rapidly when the soil sample temperature is between 0 °C and -6 °C. For M1, the unfrozen water content decreases rapidly when the soil sample temperature is between 0 °C and -7 °C. For S1, the unfrozen water content decreases rapidly when the soil sample temperature is between 0°C and -8 °C. These trends are similar to those observed in previous research [27]. The analysis results show that the speed of the decrease in unfrozen water content in this stage can reflect the pore structure and distribution in the soil mass as well as the soil's clay fraction content to a certain extent. If the soil sample has a lower clay fraction content, it can be frozen.

The unfrozen water content shows an obvious decrease with the reduction in soil sample temperature from -8 °C to -15 °C. The test results clearly show that even if the soil temperature reaches -15 °C, the unfrozen water content values in C1, M1, and S1 are 2.7%, 1.9%, and 0.4%, respectively. Thus, the unfrozen water is the bound water in soil samples, which is divided into strongly bound water and weakly bound water. The strongly bound water is difficult to freeze and will remain liquid even at the lowest freezing temperature (-83 °C) [28]. This is because the existence of strong matric suction (or molecular suction) on the bound water surface hinders liquid water's

transition to a solid state [29]. Meanwhile, the existence of matric suction makes the directional migration of conductive particles on the bound water surface and in its interior under the action of an electric field extremely difficult, thus leading to low conductivity. The silt used in this test also contains a small amount of clay particles, causing a certain degree of a “delaying” effect on the freezing process of the soil mass as well as an “inhibiting” effect on the soil mass’s conductivity.

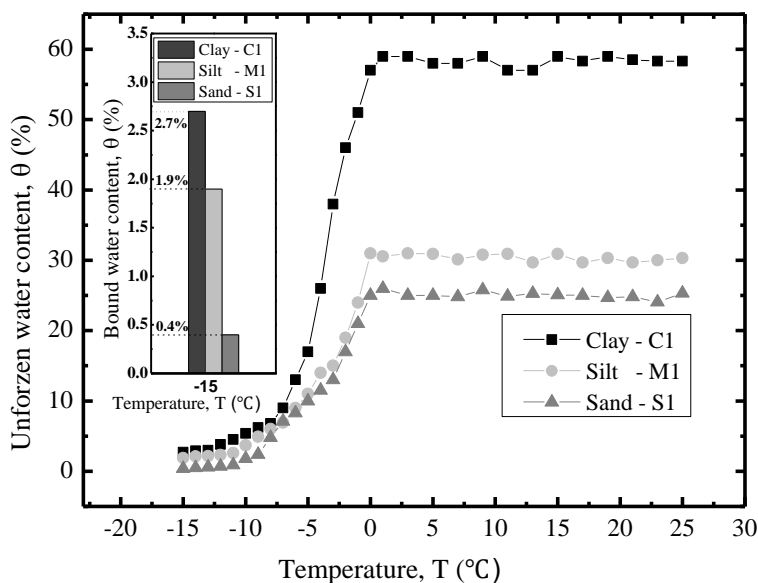


**Figure 2.** Changes in the unfrozen water content in soil during the freezing process in case of the clay, silt, and sandy soils

### 3.2. Relation between resistivity and temperature

The resistivity of sandy (S3), silt (M3), and clay (C3) soil at different temperatures is shown in Fig. 3. The thresholds of resistivity changing with temperature for C3, M3, and S3 are  $-5\text{ }^{\circ}\text{C}$ ,  $-4\text{ }^{\circ}\text{C}$ , and  $-3\text{ }^{\circ}\text{C}$ , respectively. The resistivity during the positive temperature stage basically stays unchanged with varying temperature. When the temperature is below the threshold, resistivity shows an obvious increase as temperature decreases. The reason is that the liquid water content in the samples during the positive temperature stage remains basically unchanged (Fig. 2). As a directional migration channel of conducting particles in the samples, liquid water, which can also be called a medium, largely determines the conductivity strength of a soil mass. When the sample temperature is between  $0\text{ }^{\circ}\text{C}$  and  $-5\text{ }^{\circ}\text{C}$ , resistivity shows an obvious increasing trend of between  $200\text{ }\Omega\cdot\text{m}$  and  $600\text{ }\Omega\cdot\text{m}$ ; between  $0\text{ }^{\circ}\text{C}$  and  $-4\text{ }^{\circ}\text{C}$ , resistivity shows an obvious increasing trend of between  $150\text{ }\Omega\cdot\text{m}$  and  $500\text{ }\Omega\cdot\text{m}$ ; and when the sample temperature is between  $0\text{ }^{\circ}\text{C}$  and  $-3\text{ }^{\circ}\text{C}$ , resistivity shows an obvious increasing trend of between  $100\text{ }\Omega\cdot\text{m}$  and  $450\text{ }\Omega\cdot\text{m}$ . Obviously, resistivity increases more significantly when the sample temperature reaches  $-5\text{ }^{\circ}\text{C}$  to  $-15\text{ }^{\circ}\text{C}$ , with an increased value much larger than the  $200\text{ }\Omega\cdot\text{m}$  to  $600\text{ }\Omega\cdot\text{m}$  observed at  $0\text{ }^{\circ}\text{C}$  to  $-5\text{ }^{\circ}\text{C}$  and a maximum value of more than  $9000\text{ }\Omega\cdot\text{m}$ .

The reason is that the liquid water in the soil changes into solid ice crystal particles when the temperature is between  $0\text{ }^{\circ}\text{C}$  and  $-5\text{ }^{\circ}\text{C}$ . The directional migration of conducting particles through

liquid water pore channels is inhibited by the existence of ice crystal particles, leading to an obvious decrease in soil conductivity and a corresponding rapid increase in resistivity. Although the unfrozen water content decreases from 0 °C to −5 °C, the resistivity growth rate is not the largest, with the fastest growth occurring from −5 °C to −15 °C. Further analysis shows that although the unfrozen water content decreases in this stage, that decrease is not enough to cause the directional migration channel of conducting particles to disappear completely. In other words, there is a limit value for unfrozen water content in the soil sample that can provide a directional migration channel for conducting particles. The limit value can be referred to as a temperature threshold as shown in Fig. 3. As long as the channel exists, conductivity will exist [30].

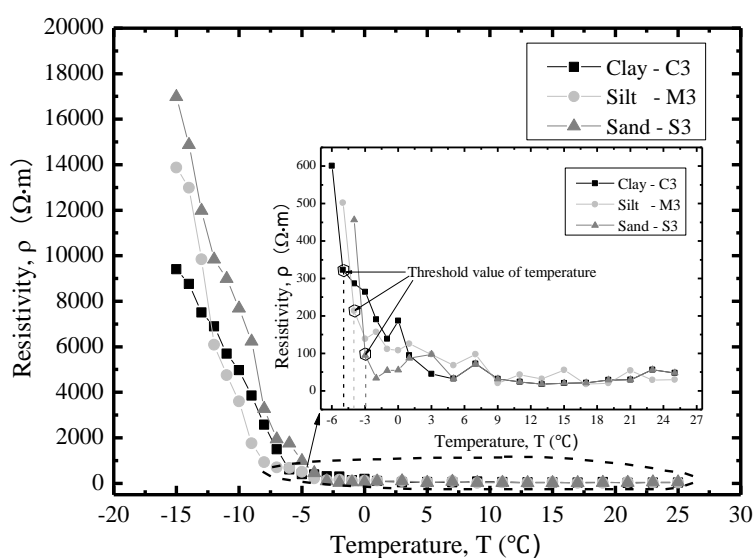


**Figure 3.** Relation between resistivity and temperature in case of the clay, silt, and sandy soils during the freezing process

### 3.3. Relation between unfrozen water content and resistivity

The relation between frozen sandy, silt, and clay soil resistivity and unfrozen water content can be obtained, as shown in Fig. 4. The resistivity value shows three different decrease trends with respect to the unfrozen water content. In stage I in Fig. 4, the resistivity value is stable; in stage II, the resistivity value increases. In stage III, the resistivity value increases quickly. The thresholds of unfrozen water content in the clay, silt, and sandy soils are 17%, 14%, and 13%, respectively. When the unfrozen water content is lower than the threshold value, the soil resistivity increases rapidly [31].

Before freezing, the total resistivity of the soil sample is stable because the water content in the inner and outer soil layers is uniform and the current is stable. In the unfrozen state, the outer soil sample cools toward freezing. During freezing, the continuous decrease in water content in the outer soil layer changes the soil–water potential. This change in the soil–water potential provides the power for water migration under freezing conditions. The suction increases near the freezing front of the

outer soil layer, resulting in the quick migration of water from the inner to the outer layer of the soil sample [32]. After migrating to the outer layer, the unfrozen water continues to freeze, and the frozen ice crystals inhibit the directional migration of the conductive ions. The high resistance of the outer parallel branches continues to increase, considerably increasing the soil resistivity. The unfrozen water in the soil is almost completely frozen at later freezing times, and the residual bound water in the soil sample cannot provide a directional migration channel for conductive ions. The thickness of the high-resistance layer in the soil sample increases drastically, and the current passes through the soil sample in series. Because the total resistance is dependent on the maximum resistance, the soil sample resistivity continues to increase.

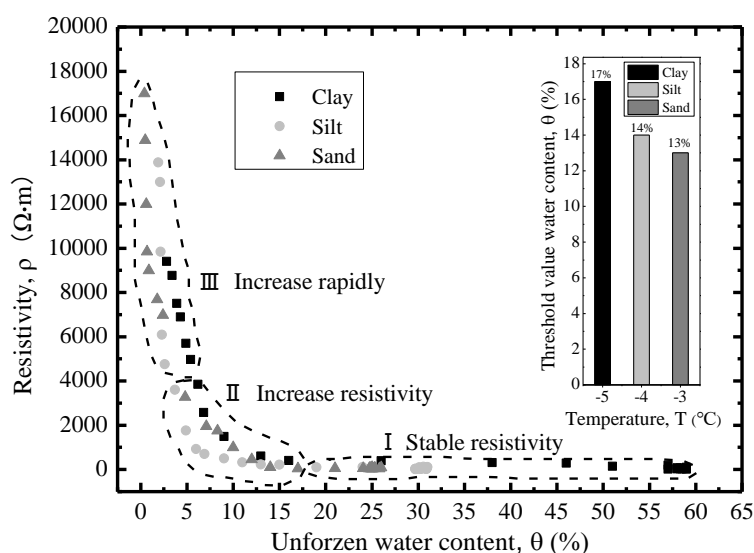


**Figure 4.** Variation in resistivity under different unfrozen water content in case of the clay, silt, and sandy soils during the freezing process

### 3.4. Relation between liquid water content and resistivity

The correlation between the drying time and liquid water content is shown in Fig. 5. The drying curves of the two parallel samples in the same group are virtually identical, thus the test has good repeatability. The relation between drying time, evaporation rate, and liquid water content of clay (C5), silt (M5), and sandy (S5) soil samples is analyzed.

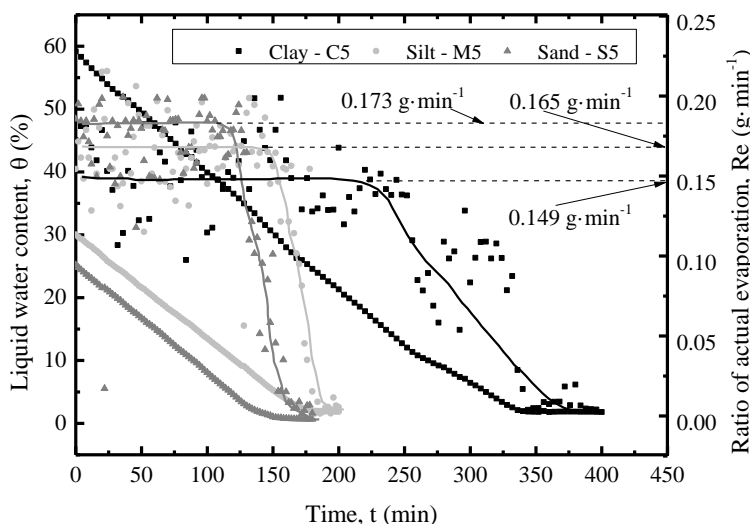


**Figure 5.** Relation between the soil mass drying time and liquid water content

The soil test sample drying can be roughly divided into a constant rate stage, a decreasing rate stage, and a residual stage. The liquid water content evaporation rates differ in the three stages. The drying time for soil samples with an initial water content of 58% is approximately 350 min at 45 °C. The drying time for soil samples with an initial water content of 30% is approximately 180 min. The drying time for soil samples with an initial water content of 25% is approximately 150 min. The evaporation rates of clay, silt, and sandy soil during the constant rate stage are 0.149 g·min<sup>-1</sup>, 0.165 g·min<sup>-1</sup>, and 0.173 g·min<sup>-1</sup>, respectively. When the evaporation rate approaches 0 g·min<sup>-1</sup>, the three soil samples have liquid water contents of approximately 2.1%, 1.5%, and 0.3%, respectively.

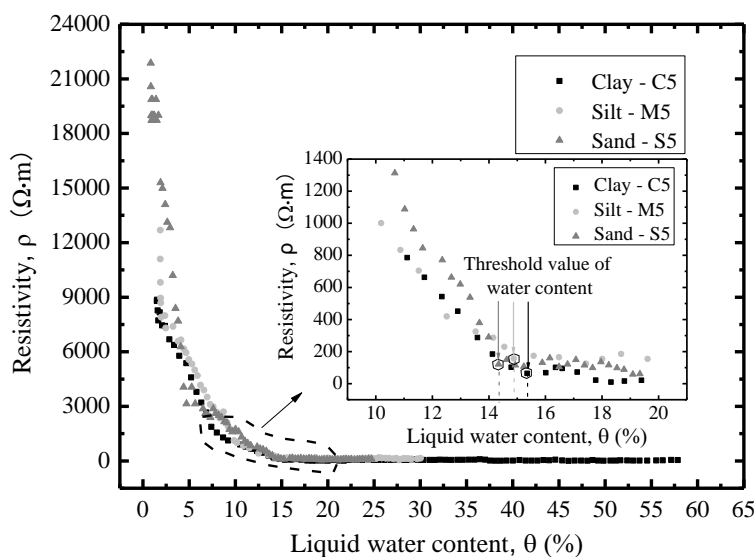


**Figure 6.** Relation between the liquid water content and resistivity

The correlation between the liquid water content and resistivity variation during the drying process is shown in Fig. 6. The overall trend of resistivity variation with liquid water content, demonstrates that the resistivity variation law can be roughly divided into a stable stage, an initial rising stage, and a fast rising stage. This law is essentially consistent with that of the unfrozen water content and resistivity of the same samples under a freezing state. The water content thresholds of clay, silt, and sandy soil are 15.35%, 14.87%, and 14.34%, respectively. When the water content is lower than the threshold, soil resistivity shows a rapid growth trend.

### 3.5. Electrochemical analysis of the unfrozen water content in frozen soil

The schematic diagram of the weakening of the conductive channel during the freezing process of the soil is shown in Fig. 7. When the soil freezes, the liquid water becomes solid ice and the ice crystals fill the free water path. The frozen soil conductivity is considerably affected by this physical process because it reduces the effect of the pore channels. The frozen soil conductivity gradually differs from the unfrozen soil conductivity as the developing ice crystals inhibit the free water path. During the continuous freezing process, the free water in the pore channels becomes completely frozen and ice crystals fill the whole free water path. The weakening effect of the pore channels becomes more obvious during this process because the free water path (the most conducive path to conductivity) is completely blocked in the frozen soil. The conducting particles can directionally migrate only through the conductive paths along the soil–particle surfaces and the soil-bound water. The soil mass conductivity is reduced significantly at this stage. Thus, liquid water is considered as the core factor affecting the soil mass conductivity.

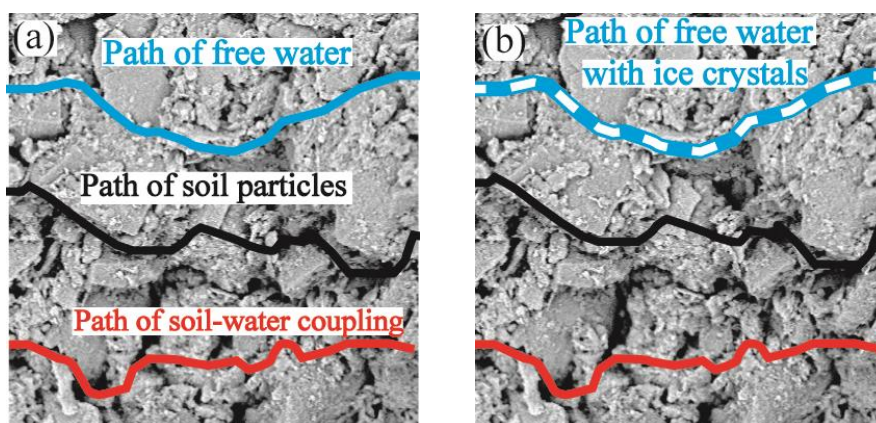


**Figure 7.** Schematic diagram of the weakening of conductive channels during the freezing process of soil

The unfrozen water behavior and the resistivity variation of freezing soil can be divided into four processes: pre-freezing, initial freezing stage, middle freezing stage, and later freezing stage. The water content and resistivity variations of the soil samples during drying are divided into four processes: pre-drying, initial drying stage, middle drying stage, and later drying stage. The unfrozen (liquid) water content in the aforementioned two sets of processes decreases inward from the outer soil layers. In the unsaturated state, the water pressures in the dried and frozen soils with the same water

content become almost identical; therefore, the soil–water potential provides similar water-migration agents during the freezing and drying processes. Because the contents and distributions of liquid (unfrozen) water in the soil are very similar in the two cases, the growth trends with respect to the soil sample resistivity are similar for the two sets of processes.

Data on the variation of liquid water content and resistivity during the drying process, as shown in Fig. 5, are analyzed. Additionally, these data are also compared with those of unfrozen water content and resistivity during freezing as shown in Fig. 3. The resistivity variation law is similar when liquid water content is decreased during the freezing and drying of soil samples. The resistivity value corresponding to the same liquid water content under freezing conditions is slightly larger than that during the drying process. The correlation between the soil resistivity and unfrozen water content during the freezing process can be expressed based on the correlation between the soil resistivity and liquid water content in the drying state.

Previous work [25] shows that the relation between the soil mass resistivity ( $\rho$ ) and unfrozen water content ( $\theta_u$ ) can be fitted by Eq. (4).

$$\rho = m\theta_u^n \quad (4)$$

where  $m$  and  $n$  are empirical parameters. Table 3 presents the coefficients of the fitting formula.

**Table 3.** Comparison of the fitting coefficients

Conditions	Types of soil	$m$	$n$	Degree of fitting
Frozen	Clay	97497	-1.862	$R^2 = 0.92$
	Silt	44195	-2.047	$R^2 = 0.94$
	Sand	9583.5	-1.561	$R^2 = 0.89$
Dry	Clay	50664	-1.598	$R^2 = 0.92$
	Silt	68345	-1.607	$R^2 = 0.81$
	Sand	42151	-1.878	$R^2 = 0.89$

Test data show that there is a certain amount of error when the correlation between the unfrozen water content and soil mass resistivity is characterized by relying solely on the relation between soil mass resistivity and liquid water content during the drying process. However, when the unfrozen water content is below the threshold, even if there is an error of  $500 \Omega \cdot m \sim 1000 \Omega \cdot m$ , which is reflected in an unfrozen water content of between 2% and 5%, that error is acceptable. The freezing and drying methods should be combined during the actual field test; however, for further cost savings, resistivity test calibration during the drying process should be preferentially adopted and assisted by the resistivity test in a partial freezing process to conduct field calibration tests.

Based on the calibrated test model, substantive tests of unfrozen water content, resistivity, and temperature as well as other physical quantities in the same kind of soil can be conducted in the laboratory. The correlation between unfrozen water content, resistivity, and temperature can also be studied economically and quickly [33]. This provides theoretical and technical support for ERT model calibration in engineering applications in cold regions.

#### 4. CONCLUSIONS

The processes and paths of decreased unfrozen water content in the soil during freezing and drying are similar, and resistivity variation is synchronous with decreased unfrozen water content in real time. During the freezing process, when the freezing temperatures of clay, silt, and sandy soil are lower than 5 °C, 4 °C, and 3 °C, respectively, the thresholds of unfrozen water content to provide directional migration channels for conducting particles are 17%, 14%, and 13%, respectively. During the drying process, the water content thresholds of clay, silt, and sandy soil are 15.35%, 14.87%, and 14.34%, respectively. When the unfrozen water content is lower than the threshold, soil resistivity shows a rapid growth trend. The correlation between the soil mass resistivity and unfrozen water content during the freezing process can be expressed by the correlation between the soil mass resistivity and liquid water content under the drying state. In other words, the theoretical model of unfrozen water can be calibrated using a resistivity test under drying. Therefore, a new calibration method can be provided for the ERT test model in engineering applications in cold regions.

#### ACKNOWLEDGEMENTS

This research is supported by the National Natural Science Foundation of China (No. 41502298), China Postdoctoral Science Foundation (No. 2016M592816), the Key Laboratory of Western Mineral Resources and Geological Engineering Ministry of Education (No. 310826161110), and the Overall Innovation Projects of Science and Technology of Shaanxi Province of China (2015KTZDSF03-07). The first author is grateful to China Scholarship Council (201708615019) for supporting the visit to the University of Alberta.

#### References

1. Z.H. Guo, Y.J. Song, X.M. Tang, and C. Wang, *Appl. Geophys.*, 15 (2018) 208.
2. N. Islami, S.H. Taib, I. Yusoff, and A.A Ghani, *Environ. Earth Sci.*, 77 (2018) 383.
3. S. Rahimi, C.M. Wood, F. Coker, T. Moody, M. Bernhardt-Barry, and B.M. Kouchaki, *Eng. Geol.*, 241 (2018) 11.
4. A. Neyamadpour, *Environ. Earth Sci.*, 78 (2019) 583.
5. W.J. Mccarter, *Geotechnique*, 34 (1984) 263.
6. J.A. Munoz-Castelblanco, J.M. Pereira, P. Delage, and Y.J. Cui, *Geotech. Test J.*, 35 (2012) 103587.
7. S.H. Jung, H.K. Yoon, and J.S. Lee, *Acta Geotech.*, 10 (2015) 275-287.
8. I. Alekseev, J. Kostecki, and E. Abakumov, *Int. Agrophys.*, 31 (2017) 1.
9. M. Keuschnig, M. Krautblatter, I. Hartmeyer, C. Fuss, and L. Schrott, *Permafrost Periglac.*, 28 (2016) 1916.
10. M.G. Drahor, *Eng. Geol.*, 252 (2019) 78.
11. G.Y. Li, Q.H. Yu, W. Ma, Z.Y. Chen, Y.H. Mu, L. Guo, and F. Wang, *Cold Reg. Sci. Technol.*, 121 (2016) 258.
12. S.Y. Li, M.Y. Zhang, W.S. Pei, and Y.M. Lai, *Appl. Therm. Eng.*, 132 (2018) 209.
13. L.Y. Tang, X.G. Wang, L. Jin, and D. Wu, *J. Test. Eval.*, 49 (2019).
14. Y.J. Shen, Y.Z. Wang, X.D. Zhao, G.S. Yang, H.L. Jia, and T.L. Rong, *Cold Reg. Sci. Technol.*, 155 (2018) 149-160.

15. S. Suzuki, *Soil Sci. Plant Nutr.*, 50 (2004) 603.
16. K. Yoshikawa, and P.P. Overduin, *Cold Reg. Sci. Technol.*, 42 (2005) 250.
17. K. Watanabe, and T. Wake, *Cold Reg. Sci. Technol.*, 252 (2009) 34.
18. X. Zhou, J. Zhou, W. Kinzelbach, and F. Stauffer, *Water Resour. Res.*, 50 (2014) 9630.
19. H. He, M. Dyck, Y. Zhao, B. Si, H. Jin, J. Lv, and J. Wang, *Cold Reg. Sci. Technol.*, 130 (2016) 33.
20. C.C. Chung, C.P. Lin, S.H. Yang, J.Y. Lin, and C.H. Lin, *Eng. Geol.*, 252 (2019) 54.
21. T. Kozłowski, *Cold Reg. Sci. Technol.*, 122 (2016) 18.
22. L. Vugmeyster, B. Hagedorn, M.A. Clark, and R.S. Sletten, *Geoderma*, (2017) 25.
23. K. Watanabe, and Y. Osada, *Cold Reg. Sci. Technol.*, 142 (2017) 79.
24. Z. Wen, W. Ma, W. Feng, Y.S. Deng, D.Y. Wang, Z.S. Fan, and C.L. Zhou, *Environ. Earth Sci.*, 66 (2012) 1467.
25. L.Y. Tang, K. Wang, L. Jin, G.S. Yang, H.L. Jia, and A. Taoum, *Cold Reg. Sci. Technol.*, 153 (2018) 55.
26. G.W. Wilson, D.G. Fredlund, and S.L. Bartour, *Can. Geotech. J.*, 31 (1994) 151.
27. A.Y. Liu, F.J. Niu, C.C. Xia, C.Y. Bao, and H. Zheng, *Cold Reg. Sci. Technol.*, (2019) 102841.
28. M. Zhang, X. Zhang, J. Lu, W. Pei, and C. Wang, *Exp. Heat Transfer*, 32 (2019) 426-438.
29. X.Y. Song, and M.H. Wang, *Int. J. Numer. Anal. Me.*, 43 (2019).
30. S.Y. Lu, and C.Y. Lin, *Appl. Phys. A-mater.*, 74 (2002) 675-681.
31. W. Shan, Y. Liu, Z. Hu, and J. Xiao, *Cold Reg. Sci. Technol.*, 119 (2015).
32. H. Guan, D. Wang, W. Ma, Y. Mu, Z. Wen, and T. Gu, *Cold Reg. Sci. Technol.*, 110(2015), 26-31.
33. R. Cardoso, and A.S. Dias, *Eng. Geol.*, 226 (2017) 1.